# Numerical study of shear-dependent non-Newtonian fluids in compliant vessels

M. Lukáčová-Medviďová,[1*] A. Zaušková[1,2]

[1] *Institute of Numerical Simulation, Hamburg University of Technology, Hamburg*
[2] *Department of Mathematical and Numerical Analysis, Comenius University, Bratislava*

SUMMARY

The aim of this contribution is to present recent results on numerical modelling of non-Newtonian flow in compliant stenosed vessels with application in hemodynamics. We consider two models of the shear-thinning non-Newtonian fluids and compare them with the Newtonian model. For the structure problem the generalized string equation for radial symmetric tubes is used and extended to a stenosed vessel. The global iterative approach to approximate the fluid-structure interaction is used. At the end we present numerical experiments for some non-Newtonian models, comparisons with the Newtonian model and the results for hemodynamic wall parameters; the wall shear stress and the oscillatory shear index.

KEY WORDS: non-Newtonian fluids, fluid-structure interaction, shear-thinning flow, hemodynamic wall parameters, stenosis

## 1. INTRODUCTION

Description of blood flow in human arteries is a very complex process. In recent years there is a growing interest in the use of mathematical models and numerical methods arising from other fields of computational fluid dynamics in the hemodynamics, see, e.g., [3], [5], [8], [11], [13], [15], [17], [18], [19], [20], [26] just to mention some of them.

There are many numerical methods used in the blood flow simulation, which are based on the Newtonian model using the Navier-Stokes equations. This is effective and useful, especially if the flow in large arteries should be modeled. However, in small arteries blood cannot be considered as the Newtonian fluid anymore. In those cappillaries, whose diameter is comparable with the size of blood red cells, the blood is even not a homogenized continuum and more

*Correspondence to: Mária Lukáčová-Medviďová, lukacova@tu-harburg.de

Contract/grant sponsor: European Union, Contract no. DEASE: MEST-CT-2005-021122

precise models, for example mixture theories need to be used. But even in the intermediate-size vessels the non-Newtonian behavior of blood is demonstrable, see [21] and the referencies therein. In fact, blood is a complex rheological mixture showing several non-Newtonian properties, for example shear-thinning or viscoelasticity [25], yield stress, stress relaxation [21]. The aim of this paper is to report on recent results concerning numerical modelling of shear-thinning flow in moving vessels with application in hemodynamics. We address the significance of non-Newtonian models for reliable hemodynamical modelling. In particular, we will show that the rheological properties of fluid have an influence on the wall deformation as well as on the hemodynamical wall indices, such as the wall shear stress and oscillatory shear index even in the intermediate-size vessels.

Consider a two-dimensional fluid motion governed by the momentum and the continuity equation

$$\begin{aligned} \rho\partial_t \boldsymbol{u} + \rho\,(\boldsymbol{u}\cdot\nabla)\,\boldsymbol{u} - \operatorname{div}\left[2\mu(|D(\nabla\boldsymbol{u})|)D(\nabla\boldsymbol{u})\right] + \nabla p &= 0 \\ \operatorname{div}\boldsymbol{u} &= 0 \end{aligned} \tag{1}$$

with $\rho$ denoting the constant density of fluid, $\boldsymbol{u} = (u_1, u_2)$ the velocity vector, $p$ the pressure, $D(\nabla\boldsymbol{u}) = \frac{1}{2}(\nabla\boldsymbol{u} + \nabla\boldsymbol{u}^T)$ the symmetric deformation tensor and $\mu$ the viscosity of the fluid. The computational domain

$$\Omega(\eta) \equiv \{(x_1, x_2, t) :\ 0 < x_1 < L,\ 0 < x_2 < R_0(x_1) + \eta(x_1, t),\ 0 < t < T\}$$

is given by a reference radius function $R_0(x_1)$ and the unknown free boundary function $\eta(x_1, t)$ describing the domain deformation. In this work we restrict ourselves to 2D domains. The fluid and the geometry of the computational domain are coupled through the following Dirichlet boundary condition

$$u_2(x_1, x_2, t) = \frac{\partial\eta(x_1, t)}{\partial t}, \quad u_1(x_1, x_2, t) = 0 \quad \text{on } \Gamma^w, \tag{2}$$

where $\Gamma^w = \{(x_1, x_2);\ x_2 = R_0(x_1) + \eta(x_1, t), x_1 \in (-L, L)\}$ is the deforming part of the boundary. With $\boldsymbol{N}$ we denote the unit outward normal vector to this boundary, $\boldsymbol{N} := (-\partial_{x_1}(R_0 + \eta), 1))/\sqrt{(\partial_{x_1}(R_0 + \eta))^2 + 1}$. Moreover, the normal component of the fluid stress tensor provides the forcing term for the deformation equation of the free boundary $\eta$, that will be introduced below.

In what follows we describe non Newtonian models that model the shear thinning properties of blood.

## 2. NON-NEWTONIAN MODELS FOR FLUID, CONTROL QUANTITIES

In the literature various non-Newtonian models for the blood flow can be found. In this paper we consider the so-called Carreau model [25] and the Yeleswarapu model [25]. According to the Carreau model for the shear-thinning fluid, the viscosity function depends on the deformation tensor in the following way

$$\mu = \mu(D(\nabla\boldsymbol{u})) = \mu_\infty + (\mu_0 - \mu_\infty)(1 + |\gamma D(\nabla\boldsymbol{u})|^2)^q \tag{3}$$

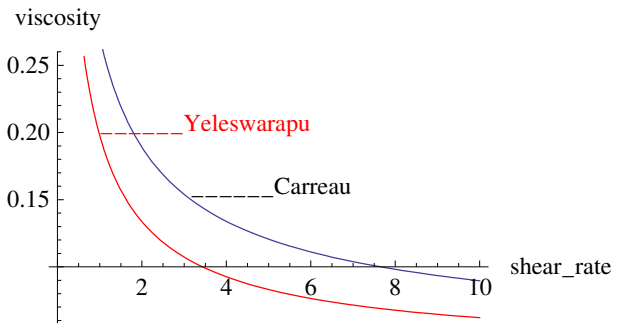


Figure 1. Viscosity function for both shear dependent models

for some given constants $q, \mu_0, \mu_\infty, \gamma$. According to [25] the physiological values for the blood are $\mu_0 = 0.56,\ \mu_\infty = 0.0345,\ \gamma = 3.313,\ q = -0.322$. Note that in the case $q = 0$ the model reduces to the linear Newtonian model used in the Navier-Stokes equations.

The Yeleswarapu model reads

$$\mu = \mu(D(\nabla \boldsymbol{u})) = \mu_\infty + (\mu_0 - \mu_\infty)\frac{\log(1 + \gamma|D(\nabla \boldsymbol{u})|) + 1}{(1 + \gamma|D(\nabla \boldsymbol{u})|)}. \tag{4}$$

The physiological measurements give $\mu_0 = 0.736,\ \mu_\infty = 0.05,\ \gamma = 14.81$ [25].

Several physical quantities have been proposed in literature in order to measure the risk zones in blood vessel. They have been introduced to describe some mechanisms correlated to intimal thickening of vessel wall. Many observations show that one reason is the blood flow oscillations during the diastolic phase of every single heath beat. To identify the occluision risk zones the *Oscillatory Shear Index*, is usually studied in literature, see [19]

$$OSI := \frac{1}{2}\left(1 - \frac{\int_0^T \tau_w \, dt}{\int_0^T |\tau_w| \, dt}\right), \tag{5}$$

where $[0, T)$ is the time interval of a single heart beat ($T \approx 1sec$) and $\tau_w$ is the *Wall Shear Stress* ($WSS$) defined as

$$WSS := \tau_w = -\mathbf{T}_f \boldsymbol{N} \cdot \boldsymbol{\tau}, \tag{6}$$

where $\mathbf{T}_f$ is the Cauchy stress tensor of fluid $\mathbf{T}_f = -p\mathbf{I} + 2\mu(|D(\nabla \boldsymbol{u})|)D(\nabla \boldsymbol{u})$, $\boldsymbol{N}$ and $\boldsymbol{\tau}$ are the unit outward normal and the unit tangential vector on the arterial wall $\Gamma^w$, respectively. $OSI$ index measures the temporal oscillations of the shear stress pointwisely without taking into account the shear stress behavior in an immediate neighborhood of a specific point.

## 3. WALL DEFORMATION MODEL

The aim of this paper is to study influence of stenotic regions in blood vessels. For this purpose we extend the *generalized string model* for vessel wall deformation [16]. We consider a 3D radially symmetric tube, see Fig. 2. We assume to have deformations only in the radial direction and set $x_1 = z$-direction and $x_2 = r$-radial direction.

The radial wall displacement, constant with respect to the angle $\theta$ is defined as difference

$$\eta(z,t) = R(z,t) - R_0(z),$$

where $= R(z,t)$, $R_0(z)$ are the actual and the reference radius of the tube, respectively. The assumption of radial geometry allow us to approximate the length of arc $dc \approx Rd\theta$, see Fig. 2 and also [16]. We assume also the small deformation gradient of displacement $(\partial_z\eta, \partial_\theta\eta)$, which implies the linear constitutive law (linear elasticity) of the vessel wall. The wall of tube is assumed to be small and constant. Moreover we approximate the infinitesimal surface in the following way $S \approx dc\, dl$.

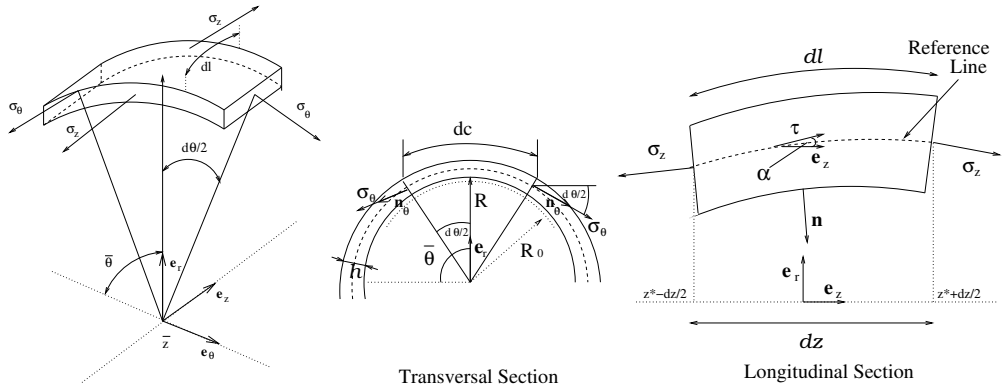


Figure 2. Small portion of vessel wall with physical characteristics, see also [16]

The linear momentum law $Force = mass \times acceleration$ is applied in the radial direction to obtain the equation for $\eta$.

$$mass = \rho_w h dc dl, \qquad acceleration = \frac{\partial^2 R(z,t)}{\partial t^2} = \frac{\partial^2 \eta(z,t)}{\partial t^2}, \tag{7}$$

where $\rho_w$ is the density of the wall and $h$ its thickness. The tissue surrounding the vessel wall interacts with the vessel wall by exerting a constant pressure $P_w$. The forces from the fluid are represented by the Cauchy stress tensor. The resulting force along the radial direction (by recalling the principle of action and reaction) is

$$f_{ext} = \boldsymbol{f}_{ext}\cdot\boldsymbol{e}_r \approx (-\mathbf{T}_f - P_w\mathbf{I})\boldsymbol{N}\cdot\boldsymbol{e}_r \frac{R}{R_0}\sqrt{1+(\partial_z R)^2}\, dc dl = (\mathbf{T}_f + P_w\mathbf{I})\boldsymbol{n}\cdot\boldsymbol{e}_r \frac{R}{R_0} dc dl,$$

where $\boldsymbol{N} = \frac{1}{\sqrt{1+(\partial_z R)^2}}(-\partial_z R, 1)$ is the unit outward normal to the boundary $\Gamma^w$ and $\boldsymbol{n} = -\boldsymbol{N}\sqrt{1+(\partial_z R)^2}$. The term $\frac{R}{R_0}\sqrt{(1+(\partial_z R)^2)}$ comes from the transformation of the curve $\Gamma^w$ to the line $(-L, L)$.

The internal forces acting on the vessel portion are due to the circumferential stress $\sigma_\theta$ (constant with respect to the angle) and the longitudinal stress $\sigma_z$. Both stresses are directed along the normal to the surface to which they act. We have $f_{int} = (\boldsymbol{f}_\theta + \boldsymbol{f}_z)\cdot \boldsymbol{e}_r$ and

$$\begin{aligned}
\boldsymbol{f}_\theta \cdot \boldsymbol{e}_r &= \Big[\sigma_\theta\Big(\bar\theta + \frac{d\theta}{2}\Big) + \sigma_\theta\Big(\bar\theta - \frac{d\theta}{2}\Big)\Big]\cdot \boldsymbol{e}_r h\ dl = 2|\sigma_\theta| cos\Big(\frac{\pi}{2} + \frac{d\theta}{2}\Big) h\ dl \\
&= -2|\sigma_\theta| \sin\left(\frac{d\theta}{2}\right) h\, dl \approx -|\sigma_\theta| h\ d\theta\, dl = -E\frac{\eta}{R_0} h\ d\theta\, dl, \\
\boldsymbol{f}_z \cdot \boldsymbol{e}_r &= \Big[\sigma_z\Big(z^* + \frac{dz}{2}\Big) + \sigma_z\Big(z^* - \frac{dz}{2}\Big)\Big]\cdot \boldsymbol{e}_r h\ dc \\
&= \frac{\tau(z^* + \frac{dz}{2}) - \tau(z^* - \frac{dz}{2})}{dz}\cdot \boldsymbol{e}_r h|\sigma_z|\, dz\, dc \\
&\approx |\sigma_z|\Big[\frac{d\tau}{dz}(z^*)\Big]\cdot \boldsymbol{e}_r h\, dz\, dc \\
&= -\left(\frac{\partial^2\eta}{\partial z^2} + \frac{\partial^2 R_0}{\partial z^2}\right)\left[1 + \left(\frac{\partial R_0}{\partial z}\right)^2\right]^{-1} \boldsymbol{n}\cdot \boldsymbol{e}_r |\sigma_z| h dz\, dc.
\end{aligned}$$

Here we have used the following properties. According to the linear elasticity assumption the stress tensor $\sigma_\theta$ is proportional to the relative circumferential prolongation, i. e.

$$\sigma_\theta = E\frac{2\pi(R - R_0)}{2\pi R_0} = E\frac{\eta}{R_0}, \quad E \text{ is Young's modulus of elasticity.}$$

To evaluate the longitudinal force we have used the following result, that is a generalization of Lemma C.1 in [16].

**Lemma.** *If $\frac{\partial\eta}{\partial z}$ is small then*

$$\frac{d\tau}{dz}(z^*) = -\left(\frac{\partial^2\eta}{\partial z^2} + \frac{\partial^2 R_0}{\partial z^2}\right)\left[1 + \left(\frac{\partial R_0}{\partial z}\right)^2\right]^{-1} \boldsymbol{n}.$$

*Proof:* Let a parametric curve $\mathbf{c}$ be defined at each $t$ on the plane $(z, r)$ by

$$\mathbf{c} : \mathbb{R} \to \mathbb{R}^2,\ z \to (c_1(z), c_2(z)) = (z, R(z,t)) = (z, R_0(z,t) + \eta(z,t)),$$

and $\tau$, $\boldsymbol{n}$, $\kappa$ denote the tangent, the normal and the curvature of $\mathbf{c}$. Then according to the Serret-Frenet formula [16] we have

$$\frac{d\tau}{dz}(z) = \left|\frac{d\mathbf{c}}{dz}(z)\right| \kappa(z)\tilde{\boldsymbol{n}}(z).$$

Here $\tilde{\boldsymbol{n}} = \pm\boldsymbol{n}$ is the normal oriented towards the center of the curve. Furthermore we have

$$\begin{aligned}\left|\frac{d\mathbf{c}}{dz}(z)\right| &= \left[1+\left(\frac{\partial R}{\partial z}\right)^2\right]^{1/2} \approx \left[1+\left(\frac{\partial R_0}{\partial z}\right)^2\right]^{1/2},\\ \kappa &= \left|\frac{dc_1}{dz}\frac{d^2c_2}{dz^2}-\frac{dc_2}{dz}\frac{d^2c_1}{dz^2}\right|\left|\frac{d\mathbf{c}}{dz}\right|^{-3} = \left|\frac{\partial^2 R}{\partial z^2}\right|\left[1+\left(\frac{\partial R}{\partial z}\right)^2\right]^{-\frac{3}{2}}\\ &\approx \left|\frac{\partial^2 R_0+\partial^2\eta}{\partial z^2}\right|\left[1+\left(\frac{\partial R_0}{\partial z}\right)^2\right]^{-\frac{3}{2}}.\end{aligned}$$

Since the sign of $\frac{\partial^2 R}{\partial z^2}$ determines the convexity of curve, $\tilde{\boldsymbol{n}} = -sign\left(\frac{\partial^2 R}{\partial z^2}\right)\boldsymbol{n}$, we obtain the desired result. ■

By summing up all contribution of balancing forces we have from the linear momentum law

$$\left\{\rho_w h R\frac{\partial^2\eta}{\partial t^2}+|\sigma_z|\frac{\left(\frac{\partial^2\eta}{\partial z^2}+\frac{\partial^2 R_0}{\partial z^2}\right)}{\left[1+\left(\frac{\partial R_0}{\partial z}\right)^2\right]}\boldsymbol{n}\cdot\boldsymbol{e}_r R h\frac{dz}{dl}+\frac{Eh\eta}{R_0}-(\mathbf{T}_f+P_w\mathbf{I})\boldsymbol{n}\cdot\boldsymbol{e}_r\frac{R^2}{R_0}\right\}d\theta\,dl = \mathcal{O}(d\theta dl).$$

Note that $\boldsymbol{n}\cdot\boldsymbol{e}_r = -1$ and $\frac{dz}{dl} \approx \cos(\measuredangle(\boldsymbol{e}_z,\tau)) = \boldsymbol{e}_z\cdot\tau/|\tau| \approx 1/\sqrt{1+\partial_z R_0}$, see Fig. 2. Thus by dividing the former equation by $\rho_w h\, R\, d\theta\, dl$ and passing to the limit for $d\theta \to 0$, $dl \to 0$ we obtain the so called *vibrating string model*. By adding the damping term $-c\partial^3_{tzz}\eta$, $c > 0$ at the left hand side we get the *generalized string model* for cylindrical geometry with a non-constant reference radius $R_0(z)$

$$\frac{\partial^2\eta}{\partial t^2}-\frac{|\sigma_z|}{\rho_w}\frac{\left(\frac{\partial^2\eta}{\partial z^2}+\frac{\partial^2 R_0}{\partial z^2}\right)}{\left[1+\left(\frac{\partial R_0}{\partial z}\right)^2\right]^{3/2}}+\frac{E\eta}{\rho_w(R_0+\eta)R_0}-c\frac{\partial^3\eta}{\partial t\partial^2 z} = \frac{(\mathbf{T}_f\boldsymbol{n}\cdot\boldsymbol{e}_r-P_w)}{\rho_w h}\frac{R}{R_0}. \quad (8)$$

## 4. REMARK ON THEORETICAL RESULTS

For the above described fluid flow problem on deforming domain with the shear dependent viscosity the existence and uniqueness result is proven in [12] for a domain, that moves according to an a-priori known domain deformation function $h \in W^{1,\infty}((0,T)\times(0,L))$. This existence result was obtained for shear thinning

Carreau-Yasuda fluids (3) with the power $q = \frac{p-2}{2}$, $p \geq \frac{1+\sqrt{5}}{2}$; the uniqueness is proven for shear thickening case $p \geq 2$.

The proof in [12] is a generalization of the previous result for Newtonian fluids in moving domains [26], [6]. In [12] the theory of monotonous operators has been applied for additional non-linear viscous term. In [6] as well as in [12] the existence and uniqueness is proven on a-priori known domain $\Omega(h)$ for a pseudo-compressible and $\kappa$-approximated system of equations in the first step. The $\kappa$-approximation comes from the following splitting of the interface condition (2), (8): the right hand side of the deformation equation (8) is replaced by $\kappa(v_2 - \partial_t \eta)$, on the other hand the Neumann boundary condition on $\Gamma^w$ (the right hand side of (8)) is equal to $\kappa(v_2 - \partial_t \eta)$ as well. Note that the interface condition (2) will be fulfilled if $\kappa \to \infty$. After proving the existence and uniqueness on $\Omega(h)$ for pseudo compressible fluid with $\kappa$-approximation of the interface condition, the existence for original fluid-structure interaction problem is obtained by letting $\kappa \to \infty$, however only on $\Omega(R_0 + \eta^k) = \Omega(h)$, i.e., in one iteration step with respect to the domain deformation.

Finally, the convergence of $\eta^{(k)} \to \eta$ for $k \to \infty$ is shown for a special case of deformation equation and for the pseudo-compressible and $\kappa$-approximated system of equations. To prove the convergence of domain deformation for the problem with the original interface condition (2), (8) stays still an open problem.

## 5. NUMERICAL METHODS

### *5.1. The decoupling method for fluid-structure interaction: the global iterative method*

The coupling between the fluid and the domain is twofold. First, the stress tensor of the fluid influences the domain deformation since it appears on the right-hand side of the structure equation (8). On the other hand, the Dirichlet boundary condition (2) on $\Gamma^w$ is related to the domain deformation $\eta$.

The fluid-structure interaction given by conditions (2) and (8) is decoupled by a *global iteration with respect to the domain geometry*. It means that in the $k$-th iteration, the vector $(\boldsymbol{u}^k, p^k, \eta^k)$ is obtained as a solution of (1) for all $(x,t) \in \Omega(\eta^{(k-1)})$, and (8) for all $x_1 \in (L, L)$. Instead of condition (2) we use

$$u_2(x_1, R_0 + \eta^{k-1}, t) = \frac{\partial \eta^{k-1}}{\partial t} = u_2^{grid},\ u_1 = 0, \qquad \text{on } \Gamma^w, \tag{9}$$

where $\boldsymbol{u}^{grid}$ is the velocity of the mesh movement related to smoothing the grid after moving its boundary (we allow just movement in the $x_2$ direction, $x_1$ direction is neglected), see also [26].

Further we linearize the equation (8) replacing the non-linear term on its left hand side by $E\eta/(\rho_w(R_0+\eta^{k-1})R_0)$. In order to decouple (1) and (8) we evaluate the forcing term at the right hand side of (8) at the old time step $t^{n-1}$, see also Fig 4. Convergence of this global method was verified experimentally. Our

extensive numerical experiences show fast convegence of domain deformation, two iteration of domain deformation differ about $10^{-4}cm$ (for e.g., $R_0 = 1cm$) pointwisely after few, about 5 iterations, see also Fig. 3.

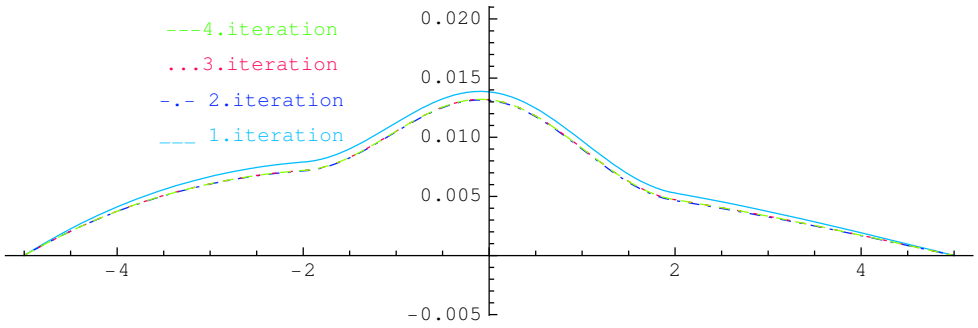


Figure 3. Convergence of global iterative method, wall deformation of a stenosed vessel at time t=0.36s, computed for physiological viscosities, $RE = 114$

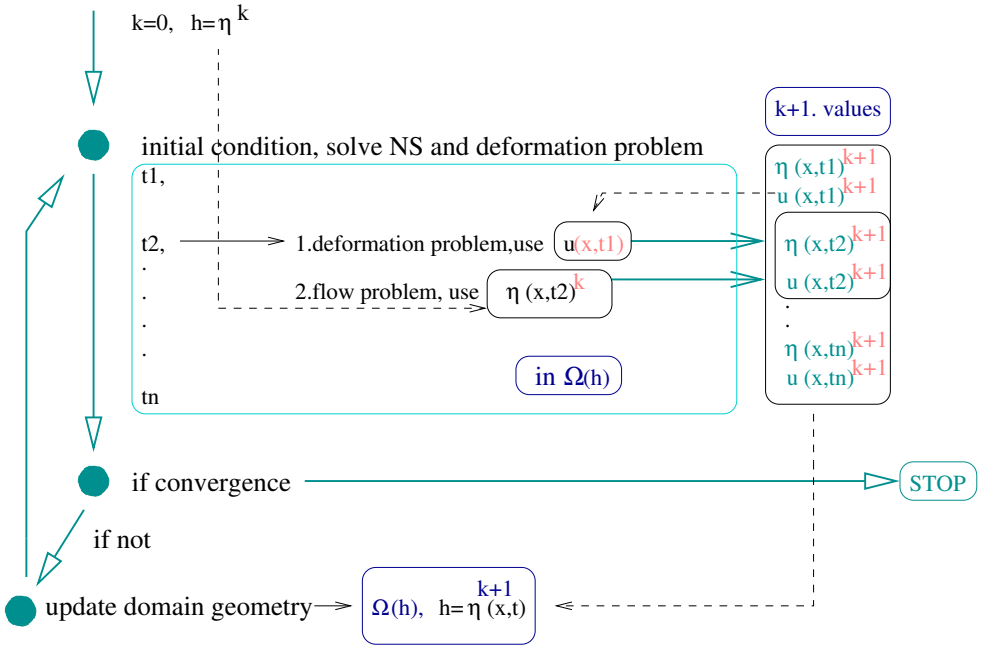


Figure 4. The sketch of the global iterative method

*5.2. Discretization methods*

For the numerical approximation of (1), (2) and (8) we have used as a basic software the UG software toolbox [1] and extended it by adding the shear-dependent viscosity as well as by adding the solver for the wall deformation equation (8). In UG the problem class library for the Navier–Stokes equations in moving domain is based on the ALE formulation, see [2]. The spatial discretization of the fluid equations (1) is realized by the finite volume method with the pseudo-compressibility stabilization. This stabilization results in the elliptic equation the for the pressure. The non-linear convective term is linearized by the Newton or fixed point method, see e.g., [14].

We describe our approximation methods in what follows.

*Linearization of the viscous term:* According to Taylor's expansion we have

$$\begin{aligned}\mu(|D(\nabla \boldsymbol{u})|)D(\nabla \boldsymbol{u}) &= \mu(|D(\nabla \boldsymbol{u}^{old})|)D(\nabla \boldsymbol{u}^{old}) \\ &+\frac{d\left[\mu(|D(\nabla \boldsymbol{u})|)D(\nabla \boldsymbol{u})\right]}{d(\nabla \boldsymbol{u})}(\nabla \boldsymbol{u}^{old})(\nabla \boldsymbol{u}-\nabla \boldsymbol{u}^{old})+\mathcal{O}((\nabla \boldsymbol{u}-\nabla \boldsymbol{u}^{old})^2),\end{aligned} \tag{10}$$

where

$$\begin{aligned}&\frac{d\left[\mu(|D(\nabla \boldsymbol{u})|)D(\nabla \boldsymbol{u})\right]}{d(\nabla \boldsymbol{u})}(\nabla \boldsymbol{u}^{old}) \\ &\qquad=\mu(|D(\nabla \boldsymbol{u}^{old})|)\frac{1}{2}(I+I^T)+\frac{d\,\mu(|D(\nabla \boldsymbol{u})|)}{d\nabla \boldsymbol{u}}(\nabla \boldsymbol{u}^{old})D(\nabla \boldsymbol{u}^{old}).\end{aligned}$$

Plugging the expression for $\frac{d[\mu(|D(\nabla \boldsymbol{u})|)\nabla \boldsymbol{u}]}{d(\nabla \boldsymbol{u})}$ into (10) and neglecting the higher order term $\mathcal{O}((\nabla \boldsymbol{u}-\nabla \boldsymbol{u}^{old})^2)$ we obtain the Newton type iteration. By neglecting the term $\frac{d\,\mu(|D(\nabla \boldsymbol{u})|)}{d(\nabla \boldsymbol{u})}(\nabla \boldsymbol{u}^{old})D(\nabla \boldsymbol{u}^{old})$ - the second term from the above expression for derivative of $\mu(|D(\nabla \boldsymbol{u})|)D(\nabla \boldsymbol{u})$ we get the fixed point iterations

$$\mu(|D(\nabla \boldsymbol{u})|)D(\nabla \boldsymbol{u})\approx \mu(|D(\nabla \boldsymbol{u}^{old})|)D(\nabla \boldsymbol{u}). \tag{11}$$

Here $(.)^{old}$ denotes the previous iteration.

In order to approximate the structure equation we apply the finite difference method. First we rewrite the second order equation (8) as a system of two first order equations. Set $\xi=\partial_t\eta$. The time discretization is realized by the following scheme

$$\begin{aligned}\frac{\xi^{n+1}-\xi^n}{\Delta t}-a\alpha\frac{\partial^2\eta^{n+1}}{\partial x_1^2} &+ b\alpha\eta^{n+1}-c\alpha\frac{\partial^2\xi^{n+1}}{\partial x_1^2} \\ &= H^n+a(1-\alpha)\frac{\partial^2\eta^n}{\partial x_1^2}-b(1-\alpha)\eta^n+c(1-\alpha)\alpha\frac{\partial^2\xi^n}{\partial x_1^2} \\ \frac{\eta^{n+1}-\eta^n}{\Delta t} &= \alpha\xi^{n+1}+(1-\alpha)\xi^n,\end{aligned}$$

where

$$a = \frac{|\sigma_z|}{\rho_w}\left[1+\left(\frac{\partial R_0(x_1)}{\partial x_1}\right)^2\right]^{-3/2}, \qquad b = \frac{E}{\rho_w(R_0+\eta)R_0} - \frac{(\mathbf{T}_f\boldsymbol{n}\cdot\boldsymbol{e}_r - P_w)}{\rho_w h R_0},$$

$$c>0, \qquad H = \frac{|\sigma_z|}{\rho_w}\left(\frac{\partial^2 R_0(x_1)}{\partial x_1^2}\right)\left[1+\left(\frac{\partial R_0(x_1)}{\partial x_1}\right)^2\right]^{-3/2} + \frac{(\mathbf{T}_f\boldsymbol{n}\cdot\boldsymbol{e}_r - P_w)}{\rho_w h}.$$

Physical meaning of quantities appearing in the coefficients $a$, $b$, $c$ is following, see [7]: the Young's modulus is $E = 0.75.10^5 dynes.cm^{-2}$, the wall thickness $h = 0.1cm$, the density of the vessel wall tissue $\rho_w = 1.1g.cm^{-3}$, $|\sigma_z| = G\kappa$, where $\kappa = 1$ is the Timoshenko's shear correction factor and $G$ is the shear modulus, $G = E/2(1+\sigma)$, where $\sigma = 1/2$ for incompressible materials. The coefficient $c = \gamma/(\rho_w h)$, we have used $\gamma = 2.10^4$.

If $\alpha = 0$ we have an explicit scheme in time, for $\alpha = 1$ we obtain an implicit scheme. The parameter $\alpha = \frac{1}{2}$ yields the Newmark scheme, which is proven to be unconditionally stable at least in the case of homogeneous Dirichlet boundary conditions, see [15].

## 6. NUMERICAL EXPERIMENTS

In this section we present a series of numerical experiments for fluid flow in a compliant vessel. The aim is to investigate differences in the behavior of Newtonian and non-Newtonian fluids in moving domains. We have chosen two non-Newtonian models for the blood flow often used in the literature, the Carreau and the Yeleswarapu model. Further, we study the influence of non-Newtonian rheology on some hemodynamical wall parameters such as the wall shear stress $WSS$ and the oscillatory shear index $OSI$.

We consider a two dimensional symmetric tube with a smooth stenosed region. Due to the symmetry we can restrict our computational domain to the upper half of the tube. A representative geometry is shown e.g., in Fig. 9. The impermeable moving wall $\Gamma^w$ is modeled as a smooth stenosed constriction given as, see [13],

$$\begin{aligned} f(x_1) &= 1 - \frac{g}{2}\left(1+\cos\left(\frac{\pi x_1}{2}\right)\right) && \text{if } x_1 \in |r| \\ f(x_1) &= 1 && \text{if } x_1 \in (-L,-r)\cup(r,L). \end{aligned}$$

We took $L = 5$, $r = 2$, $g = 0.3$. These values give a stenosis with 30% area reduction which corresponds to a relatively mild occlusion, leading to local small increment of the Reynolds number.

Let $\Gamma^{in} = \{(-L,x_2);\, x_2 \in (0,1)\}$, $\Gamma^{out} = \{(L,x_2);\, x_2 \in (0,1)\}$, $\Gamma^s = \{(x_1,0);\, x_1 \in (-L,L)\}$ denote the inflow, outflow and symmetry boundary, respectively. We prescribe the pulsatile parabolic velocity profile on the inflow boundary of the tube

$$u_1(-L,x_2) = V(R(t)^2 - x_2^2)f(t), \qquad u_2(-L,x_2) = 0, \tag{12}$$

where $f(t)$ is some temporal function modelling pulses of hearth and $R(t) = R_0(0) + \eta^k(0,t)$, $R_0(0) = 1$ and $V$ is the maximal velocity at the inflow. For temporal function $f(t)$ we consider a model function $f(t) = sin^2(\pi t/\omega)$ with the period $\omega = 1s$ as well as the iliac artery flow rate measurements, see Fig.5.

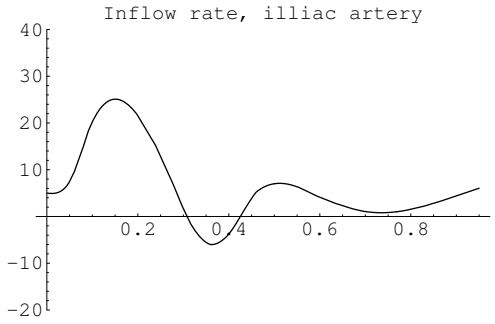


Figure 5. Inflow rate $Q(t)$ in *sec.*

The flow rate is defined as

$$Q(t) = \int_{\Gamma^{in}} u_1 dx_2.$$

By integration inflow velocity (12) over $\Gamma^{in}$ we obtain that $Q(t) = \frac{4}{3}VR(t)f(t)$. Consequently we get the relation for temporal function $f(t)$ in (12),

$$f(t) = Q(t)\frac{3}{4VR(t)}. \tag{13}$$

On $\Gamma^s$ the symmetry boundary condition $\partial_{x_1} u_1 = 0,\ u_2 = 0$ is prescribed, on $\Gamma^{out}$ the Neumann type boundary condition $-\mathbf{T}_f \boldsymbol{N} = P_{out}\mathbf{I}\boldsymbol{N}$.

Since the viscosity of the non-Newtonian fluid is a function of shear rate, see Fig. 1, we compute the Reynolds number using averaged viscosity

$$RE = \frac{\rho V l}{\frac{1}{2}(\mu_0 + \mu_\infty)},$$

where $\rho$ is the fluid density, $V$ is the characteristic velocity (maximal inflow velocity), $l$ is the characteristic length (we take the diameter of the tube). In order to take into account also the effects of assymptotical (limitting) viscosity values, we define $RE_0 = \rho V l/\mu_0$, $RE_\infty = \rho V l/\mu_\infty$ and introduce it in the Table I below as well.

In the following experiments we have chosen in analogy to Nadau and Sequeira [13], $RE_0 = 30$ or $RE_0 = 60$ and $\mu_\infty = \frac{1}{2}\mu_0$ for the Carreau model (3) as well as for the Yeleswarapu model (4). We should point out that in [13] the

authors studied similar problem, however they did not consider pulsatile flow and deforming vessel walls. They used moreover generalized Oldroyd-B model for blood. Further we have also tested the stability and robustness of the method for physiological parameters [25], see Table I.

Table I. Experimental data

| $RE_0 = 30$ | $RE_0 = 60$ | $RE_0 = 30$ | $RE_0 = 60$ |
|---|---|---|---|
| **Carreau model**<br>$q = 0,\ \ q = -0.322,\ \ q = -10$<br>$\lambda = 1$ | | **Yeleswarapu model**<br>$\lambda = 14.81$ | |
| $\mu_\infty = 1.26P$<br>$\mu_0 = 2.53P$<br>$V = 38cm.s^{-1}$<br>$RE = 40,\ RE_\infty = 60$ | $\mu_\infty = 0.63P$<br>$\mu_0 = 1.26P$<br>$V = 38cm.s^{-1}$<br>$RE = 80,\ RE_\infty = 121$ | $\mu_\infty = 1.26P$<br>$\mu_0 = 2.53P$<br>$V = 38cm.s^{-1}$<br>$RE = 40,\ RE_\infty = 60$ | $\mu_\infty = 0.63P$<br>$\mu_0 = 1.26P$<br>$V = 38cm.s^{-1}$<br>$RE = 80,\ RE_\infty = 121$ |
| physiological parameters<br>$q = -0.322\ \ \lambda = 3.313$ | | physiological parameters | |
| | $\mu_\infty = 0.0345P$<br>$\mu_0 = 0.56P$<br>$V = 17cm.s^{-1}$<br>$RE = 114,\ RE_\infty = 986$ | | $\mu_\infty = 0.05P$<br>$\mu_0 = 0.736P$<br>$V = 22.3cm.s^{-1}$<br>$RE = 113,\ RE_\infty = 892$ |

### *6.1. Experiments for model data*

In what follows we have plotted results comparing several aspects of Newtonian and non-Newtonian flow in the straight channel and in the channel with a stenotic occlusion. We chose the Dirichlet inflow boundary condition (12), which model some pulsatile parabolic velocity profile at the inflow. Here we took $f(t) = sin^2(\pi t/\omega)$, where $\omega = 1s$.

Fig. 6 describes time evolution of the wall deformation function $\eta$ at two time instances $t = 0.36s$ and $t = 0.96s$ for the straight and stenotic channel and for different non-Newtonian viscosities. Clearly, we can see effects due to the presence of stenosis in Fig. 6. The differencies in wall deformation for non-Newtonian and Newtonian ($q = 0$) fluids are not significant. Further, the wall deformation for the Yeleswarapu model and for the Carreau model with $q = -10$ are comparable. Fig. 7 describes the wall shear stress $WSS$ distribution along the upper moving wall in the stenosed channel. We compare the $WSS$ for the Newtonian and non-Newtonian fluids. Analogously as before we see that the $WSS$ depends considerably on the geometry, we observe a presence of peak in the $WSS$ due to the stenosis for both Newtonian and non-Newtonian models. The rheology of the fluid is more significant by measurements of the $WSS$; bigger differences in the $WSS$ can be seen for the non-Newtonian models in comparison with the Newtonian models, in particular at $t = 0.96s$. Also some small differences in peak behavior can be observed at this time.

Another important hemodynamic wall parameter is the oscillatory shear index

$OSI$. Fig. 8 describes the behavior of the $OSI$ for the straight and stenotic channel. We can see different effects due to the presence of stenosis in the $OSI$. Moreover the peaks in the $OSI$ are more dominant for the non-Newtonian models in comparison to the Newtonian flow. High $OSI$ values indicate the areas with the large stenotic plug danger. Fig. 8 indicates, that such areas appear at the end of stenotic reduction.

We conclude this subsection with a statement, that the fluid rheology and domain geometry may have a considerable influence on the hemodynamic wall parameters $WSS$ and $OSI$.

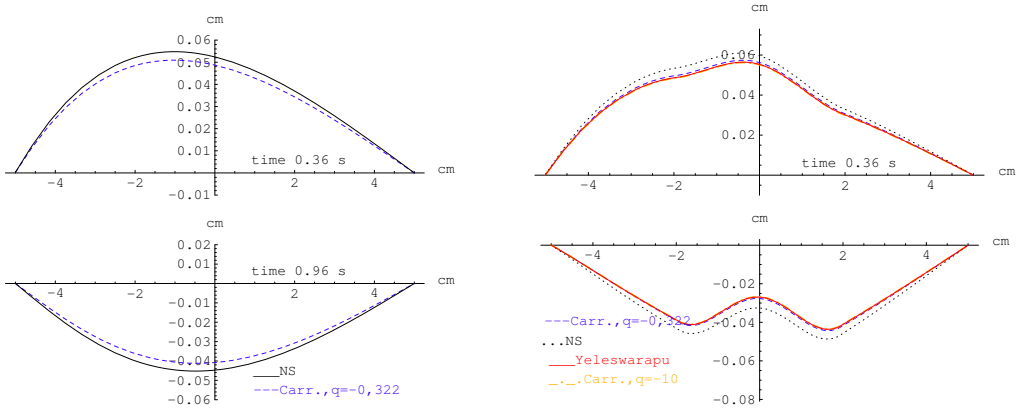


Figure 6. Wall deformation, left: the Newtonian (NS) and the Carreau models in the straight channel; right: the Newtonian (NS), the Yeleswarapu and the Carreau models in the stenosed channel, $RE = 80$

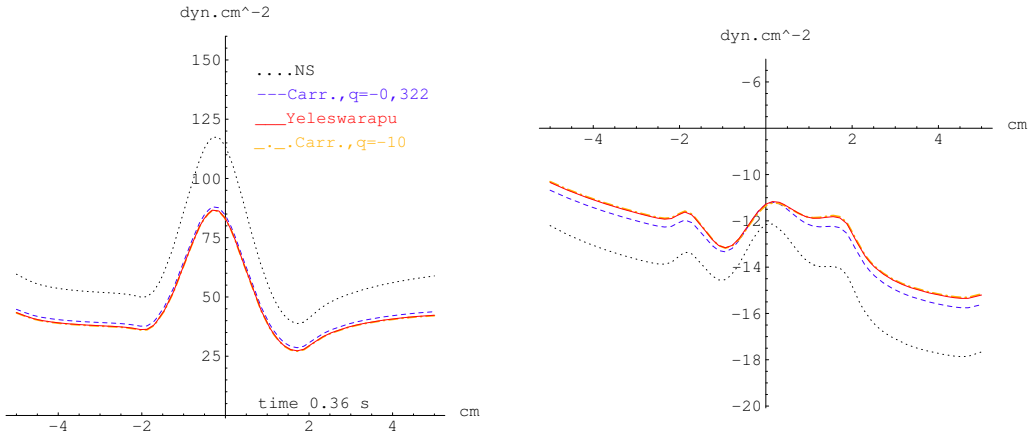


Figure 7. $WSS$: the Newtonian (NS), the Yeleswarapu and the Carreau models, $RE = 80$

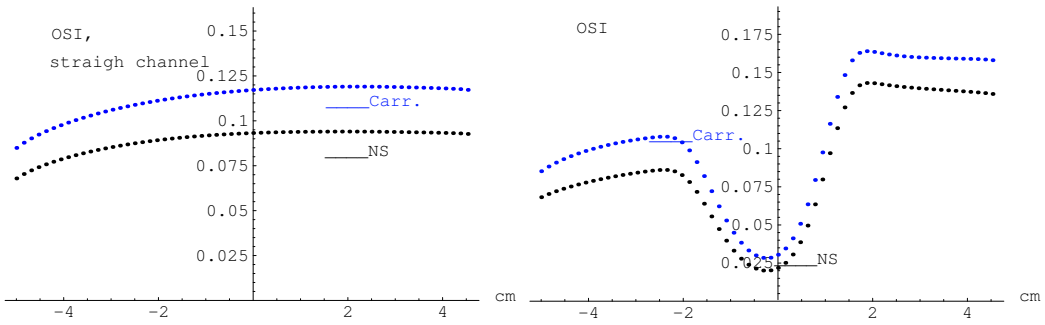


Figure 8. *OSI* indices computed using the Newtonian (NS) and the Carreau models with $q = -0.322$ in the straight channel (left) and in the stenosed channel (right), $RE = 80$

### *6.2. Experiments for physiological parameters*

We present several results comparing the behavior of both non-Newtonian models, the Carreau and the Yeleswerapu model with corresponding physiological parameters, see Table I. In the first experiment we consider the pulsatile velocity profile at the inflow as before.

Fig. 9 describes the velocity field at different times. In Fig. 10 the streamlines and the pressure distribution for the Yeleswarapu model at different time instances can be seen. At time $t = 0.96$, where the inflow velocity is decreasing we can observe reverse flow and vertices in the streamlines. Only marginal differences between the Carreau and the Yeleswerapu model are observed in the wall deformation $\eta$, Fig. 6.2. More visible differences between these two non-Newtonian models can be observed in the $WSS$ and $OSI$ indices, see Fig. 12 and Fig. 13.

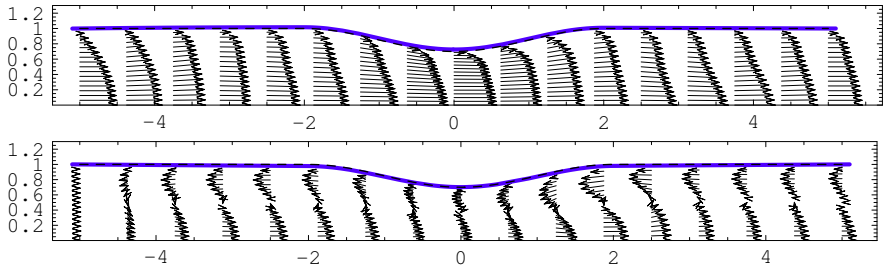


Figure 9. Physiological experiment: the Carreau model, $RE = 80, t = 0.36s$, $t = 0.96s$, velocity field

Moreover, our experiments confirm, that the differences between Newtonian and non-Newtonian fluids in the wall deformation, wall shear stress and also $OSI$ increase with increasing Reynolds numbers, see Figs. 14, 15, 16.

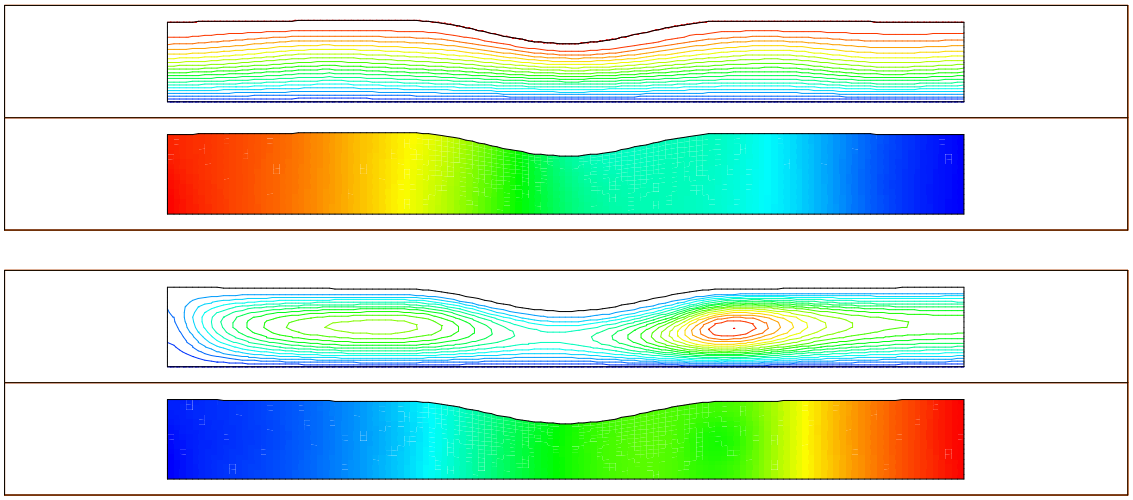

Figure 10. Physiological experiment: the streamlines and the pressure distribution for the Yeleswarapu model in two time distances, upper: $t = 0.36s$, bottom $t = 0.96$, $RE = 80$

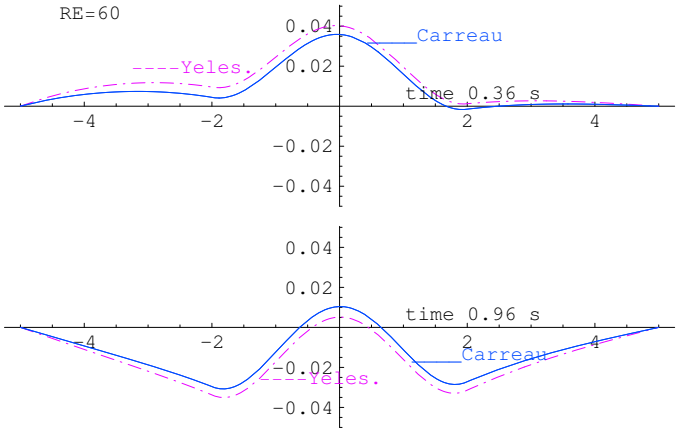


Figure 11. Physiological experiment: comparison of the wall deformation for non-Newtonian models

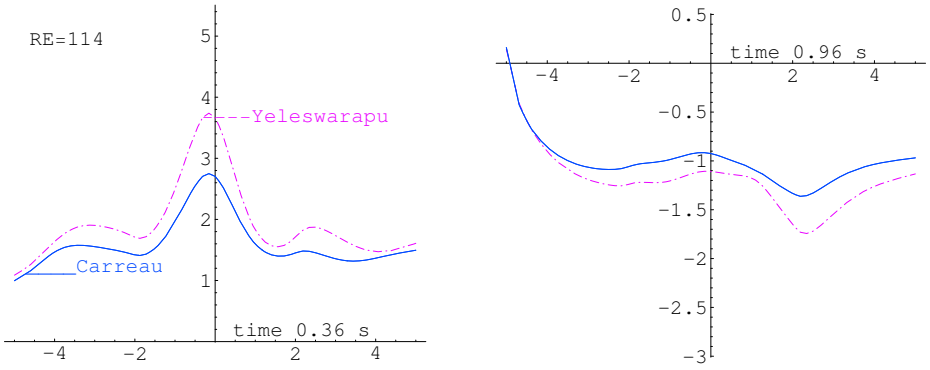


Figure 12. Physiological experiment: comparison of the $WSS$ for non-Newtonian models

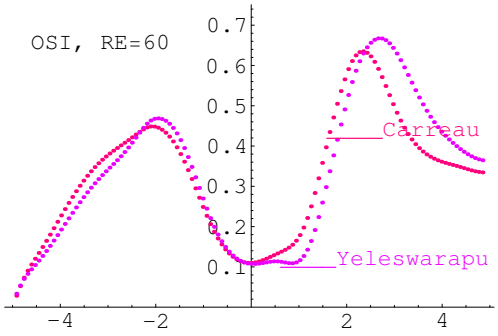


Figure 13. Physiological experiment: the $OSI$ index for non-Newtonian models

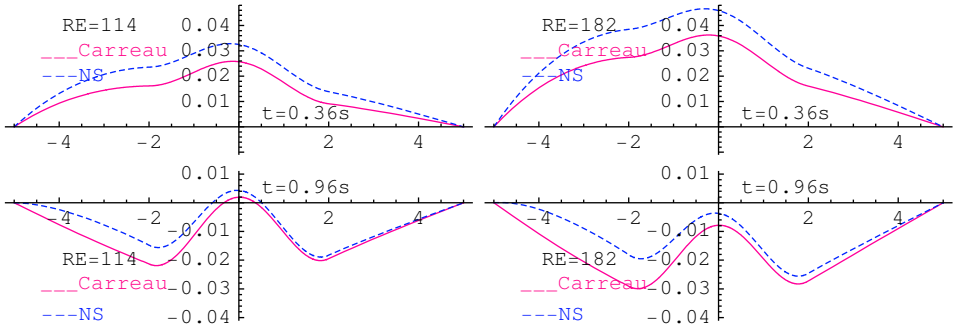


Figure 14. Physiological experiment: comparison of wall deformations for different Reynolds numbers

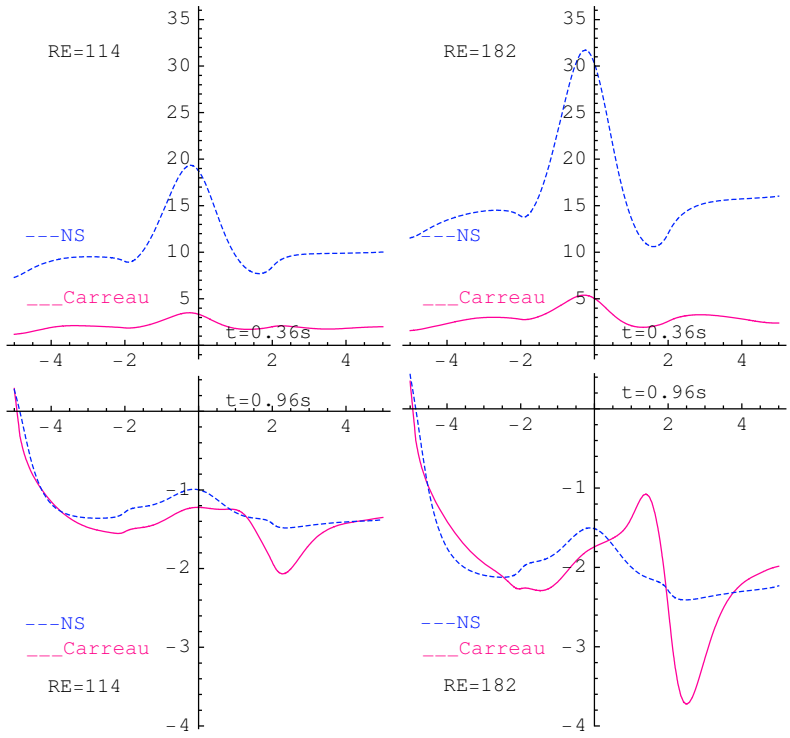


Figure 15. Physiological experiment: comparison of wall shear stresses for different Reynolds numbers

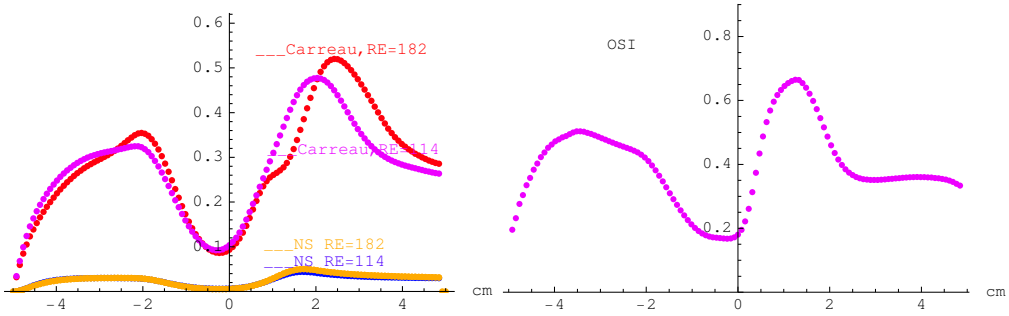


Figure 16. Physiological experiment: left: the *OSI* indices for different Reynolds numbers, right: *OSI* index for illiac artery inflow, Neumann boundary condition for $\eta$ and damping of deformation in stenotical region

In the second physiological experiment we considered the Neumann type boundary condition for deformation equation on the inflow boundary. This condition represents a free movement of vessel wall on the inflow and outflow part and seems to be more natural for modelling the flow in a part of elastic vessel. In this experiment, moreover, we introduced some damping of deformation in stenotical region. This is reasonable, since the stenotic occlusion is created by fat accumulated on the vessel wall and the stenotical plug may have different elastic properties. We considered Young's modulus $E$ and damping parameter $c$ in structure equation (8) being following functions of longitudinal variable $x$

$$E = E(x) = \begin{cases} E & x \in (-5,-2) \cup (2,5) \\ E[1 + 0.1(x^2 - 4)] & x \in \langle -2, 2 \rangle, \end{cases}$$

$$c = c(x) = \begin{cases} 20.000 & x \in (-5,-2) \cup (2,5) \\ 20.000[1 - 0.01(x^2 - 4)] & x \in \langle -2, 2 \rangle. \end{cases}$$

In order to obtain more realistic hemodynamical situation, the parabolic velocity profile at the inflow was multiplied with temporal function derived from iliac artery measurements, see Fig. 5 and (13). We set the period $T = 0.9s$ and final computational time is chosen to be $t = 1.8s$. The numerical results are presented in Figs. 16, 17, 19, 18.

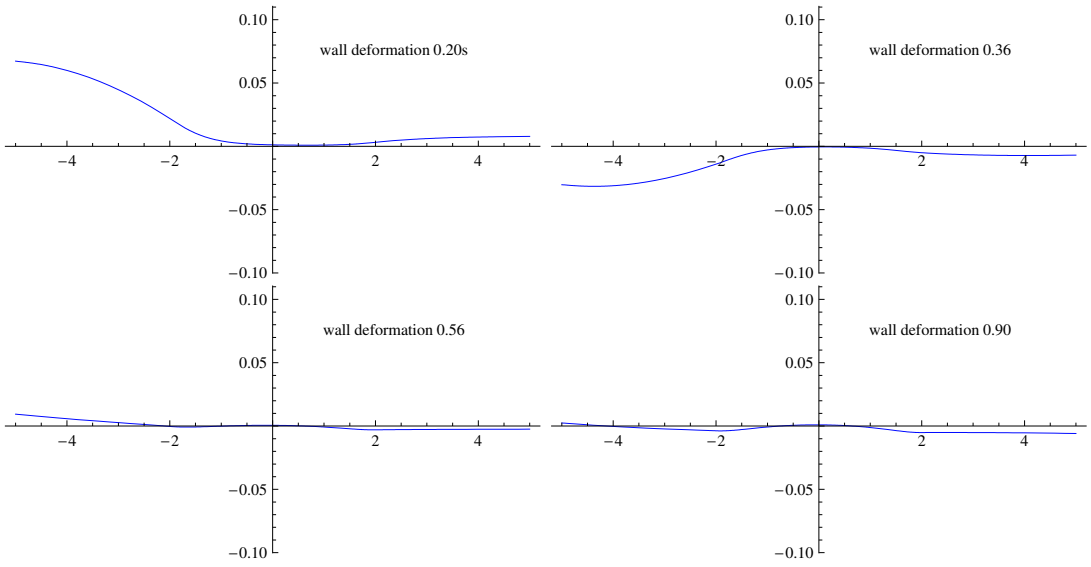


Figure 17. Physiological experiment: wall deformation at four different time instances

Notice that the vessel wall at inflow and outflow are not fixed and the radius of vessel wall is increasing and decreasing according to the acting flow forces,

Fig. 17. Due to the increased damping parameter and decreased elasticity in the stenosed area the wall deformation presented in Fig. 17 is reduced considerably in comparison to the previous experiments (e.g. Fig. 14). Effects of different elasticity behavior at the stenosed part have also considerable influence on the behavior of hemodynamical wall parameters $OSI$ and $WSS$, see Figs. 16, 18.

Comparing pictures for streamlines as well as pressure presented in Fig. 19 we see much more complex phenomena, different types of recirculation as well as flow behavior. This different flow and wall shear stress development, notice also Fig. 18, is conditioned by realistic temporal pulses at the inflow part of the vessel coming from illiac artery measurements.

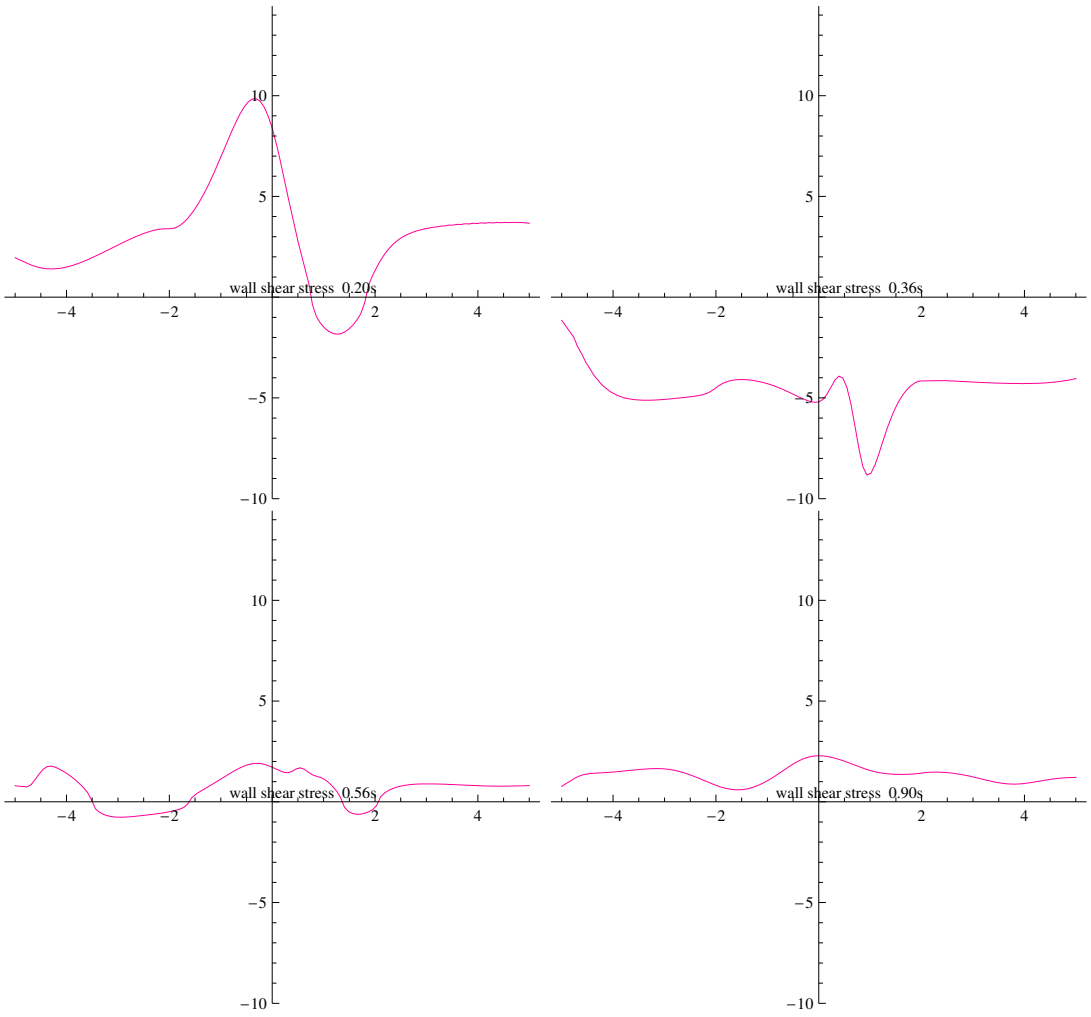


Figure 18. Physiological experiment: wall shear stress at four different time instances

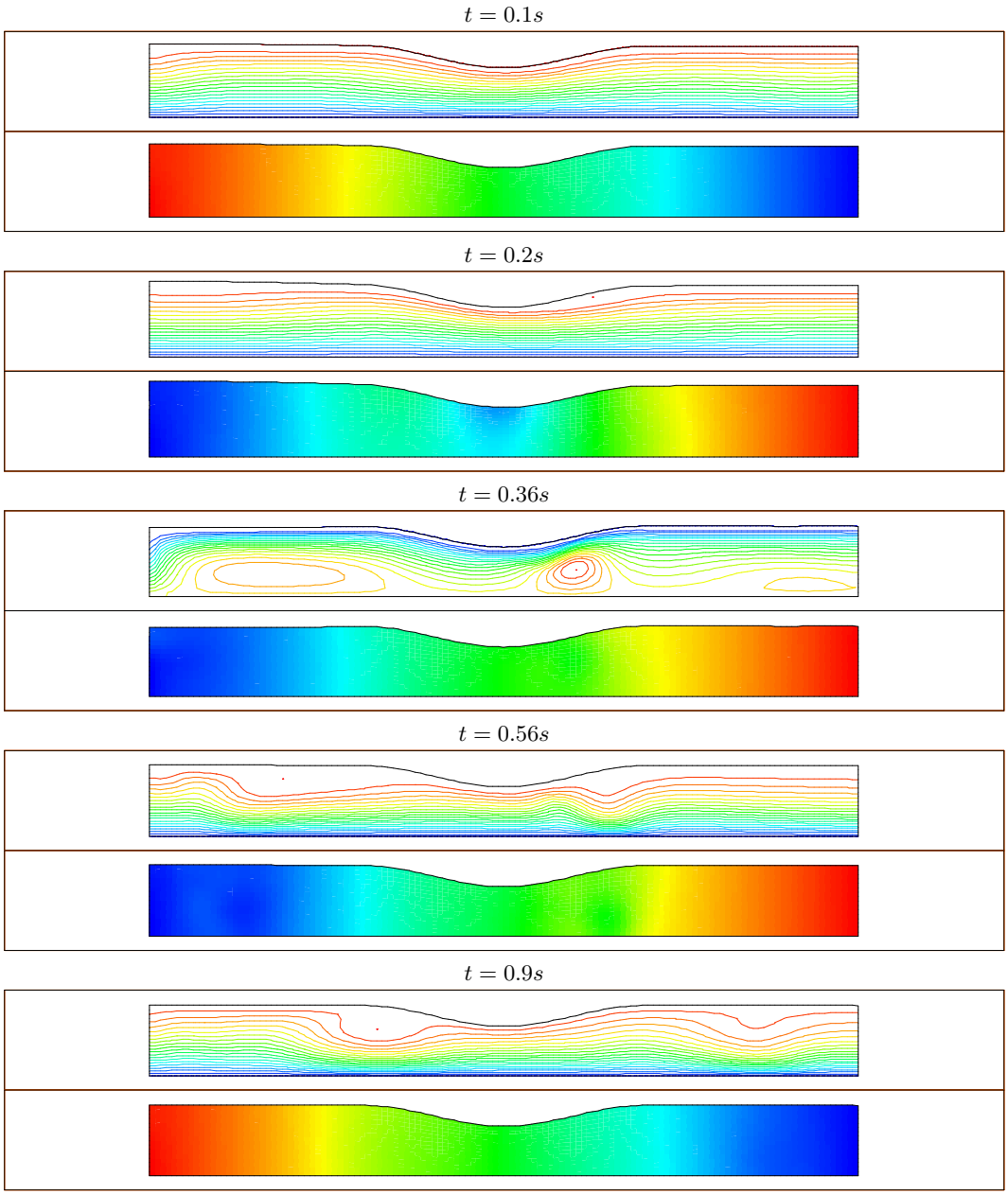


Figure 19. Physiological experiment: wall deformation at five different time steps $t = 0.1s$, $t = 0.2s$, $t = 0.36s$, $t = 0.56s$, $t = 9s$, free ends of tube, damping in the stenotical region, illiac artery inflow

## 7. CONVERGENCE STUDY

In the following we study the experimental order of convergence using $L^2$ errors of solution at different meshes, cf. e.g. in [10]

$$EOC = log_2 \frac{\|\boldsymbol{v}_h - \boldsymbol{v}_{h/2}\|_{L^2}}{\|\boldsymbol{v}_{h/2} - \boldsymbol{v}_{h/4}\|_{L^2}},$$

where $\boldsymbol{v}_h$ is the solution on the mesh with mesh size $h$. The computational domain $\Omega(\eta)$ is consequently divided into $16 \times 2$ elements (mesh 1.), $32 \times 4$ elements (mesh 2.), $64 \times 8$ elements (mesh 3.), $128 \times 16$ elements (mesh 4.), where the element size $\Delta x$ and $\Delta y$ is halved. We worked with piecewise linear approximation for fluid velocities and the backward Euler method for time discretization [1], [14], [26]. We considered stationary case for both the rigid as well as the deforming tube.

Table I. demonstrates the second order in space convergence for the Newtonian as well as non-Newtonian flow in the rigid tube, see the Fig. 20 for the geometry and boundary conditions. The non-Newtonian model (Carreau model, $\mu_\infty = 0.63,\ \mu_0 = 1.26,\ V_{inflow} = 38cm.s^1,\ q = -0.2$) is compared to Newtonian fluid ($\mu = 0.63,\ V_{inflow} = 38\, cm.s^{-1}$). On the finer meshes the effect of shear thickening is stronger at the boundary layer and may cause the reduction of the convergence in the non-Newtonian case.

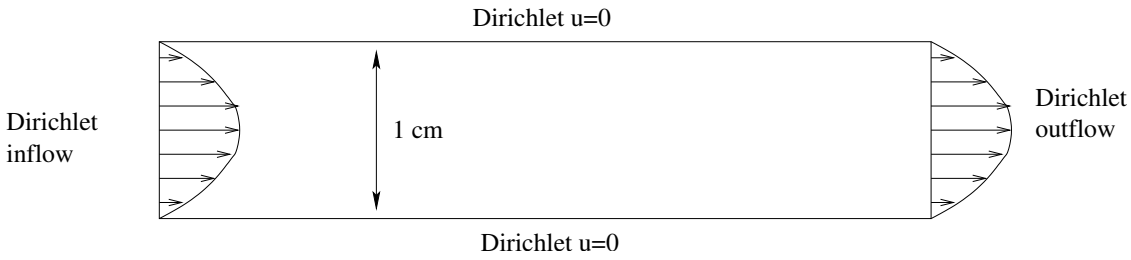


Figure 20. Boundary conditions in first experiment

In the following tables we use following notations:

$$Err(\boldsymbol{v}_h) = \|\boldsymbol{v}_h - \boldsymbol{v}_{h/2}\|_{L^2}/|\Omega|, \quad Err(\eta_h) = \|\eta_h - \eta_{h/2}\|_2$$

Table II shows convergence results for non-Newtonian as well as Newtonian fluid in rigid halved domain with symmetry condition at the central line, see Fig. 21. We can notice slightly worse second order convergence rate in the velocity, however the convergence is rapidly reduced with refining the grid especially in the non-Newtonian case. This effect is caused by using different boundary conditions (the Neumann boundary condition at the outflow and the symmetry

Table II. Convergence order in rigid tube for Newtonian and non-Newtonian fluid

| 1.exp. | | Newt. fluid $q = 0$ | | non-Newtonian fluid, $q = -0.2$ | | | | |
|---|---|---|---|---|---|---|---|---|
| mesh | $\Delta t$ | $Err(\boldsymbol{v}_h)$ | EOC | $Err(\boldsymbol{v}_h)$ | EOC | $\Delta t$ | $Err(\boldsymbol{v}_h)$ | EOC |
| 2/1 | 0.002 | 8.577022 | | 9.342948 | | 0.02 | 7.988901 | |
| 3/2 | 0.002 | 1.442296 | 2.572 | 1.502546 | 2.636 | 0.01 | 1.352937 | 2.562 |
| 4/3 | 0.002 | 0.299673 | 2.267 | 0.293375 | 2.357 | 0.002 | 0.293375 | 2.205 |

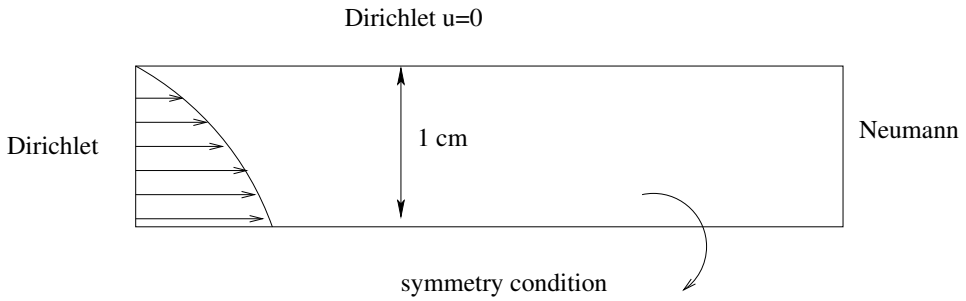


Figure 21. Boundary conditions in the second experiment

condition at the central line). Note the differences in convergence order obtained for shear-dependent-viscosity fluid and constant-viscosity fluid. For comparison the convergence order for another shear-thickening exponents are given in Table IV. Note that in the case $q = -0.1$ the convergence order on finer meshes is even worse.

Table III. Convergence order in rigid tube

| 2. exp. | | Newtonian fluid $q = 0$ | | non-Newt. fluid $q = -0.2$ | |
|---|---|---|---|---|---|
| mesh | $\Delta t$ | $Err(\boldsymbol{v}_h)$ | EOC | $Err(\boldsymbol{v}_h)$ | EOC |
| 2/1 | 0.002 | 1.078302 | | 0.985871 | |
| 3/2 | 0.002 | 0.275817 | 1.967 | 0.276619 | 1.834 |
| 4/3 | 0.002 | 0.008409 | 1.714 | 0.124013 | 1.157 |

Experiments for deforming tubes follow. We performed experiments on the halved domain with symmetry or Dirichlet boundary condition an the central line and the Neumann boundary condition at the outflow, see Fig. 21, 22. Eleven iteration of domain geometry has been performed in global framework (i.e. the values from previous domain iteration has been used in order to deform

Table IV. Convergence order in rigid tube

| 2. exp. | | non-Newt. fluid $q = -0.1$ | | non-Newt. fluid $q = -0.3$ | |
|---|---|---|---|---|---|
| mesh | $\Delta t$ | $Err(\boldsymbol{v}_h)$ | EOC | $Err(\boldsymbol{v}_h)$ | EOC |
| 2/1 | 0.002 | 0.9307086 | | 1.025074 | |
| 3/2 | 0.002 | 0.2627934 | 1.824 | 0.2806220 | 1.869 |
| 4/3 | 0.002 | 0.1207427 | 1.122 | 0.1131567 | 1.310 |

the domain in actual fluid-structure computation). In each global iteration the computational time was 0.8 sec. The stationary solution has not been obtained until the time 0.8 sec, because of small temporal oscillations of the deformation function and consequently the domain size. Therefore we compare the solution in one fixed time step $t = 0.8sec$.

Table V. Convergence order in deforming tube

| 2. exp. | | non-Newtonian fluid $q = -0.2$ | | | | domain size |
|---|---|---|---|---|---|---|
| mesh | $\Delta t$ | $Err(\boldsymbol{v}_h)$ | EOC($\boldsymbol{v}_h$) | $Err(\eta_h)$ | EOC($\eta_h$) | $\lvert\Omega(\eta_{h/2})\rvert$ |
| 2/1 | 0.002 | 1.026306 | | 0.011956 | | 3.185052 |
| 3/2 | 0.002 | 0.281130 | 1.853 | 0.005477 | 1.126 | 3.187671 |
| 4/3 | 0.002 | 0.1210801 | 1.231 | 0.002272. | 1.269 | 3.188426 |

We observe again the second order convergence for spatial discretization method for fluid problem. However, the spatial discretization method for domain deformation is only of first order. The lower convergence rate for $\eta$ as expected (we used Newmark scheme, which is of 2. order) may be caused by coupling with the velocity and pressure through the forcing term on the right hand side of deformation equation.

For comparison we have performed also experiments on halved domain with Dirichlet boundary condition on the central line of the domain, see Fig. 22. For this kind of boundary conditions we have obtain better convergence order for velocity and $\eta$ as well, however the EOC for $\eta$ is decreasing extremely with refining the grid, see the Table VI and VII for non-Newtonian as well as Newtonian fluid.

Note, that the EOC for $\eta$ in the 2. experiment (with the symmetry boundary condition at the central line) is little bit more than 1 and even increases

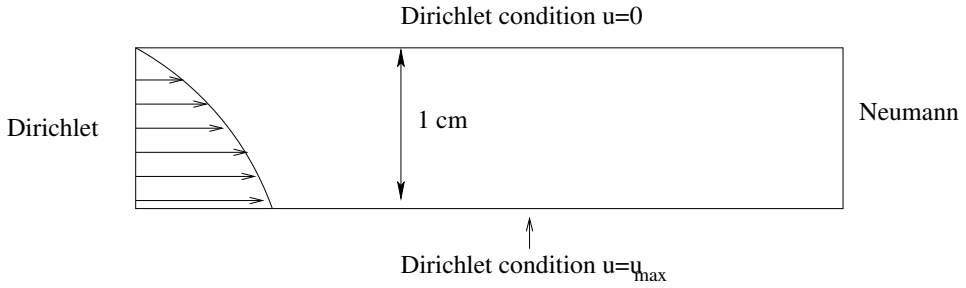


Figure 22. Boundary conditions in the third experiment

Table VI. Convergence order in deforming tube

| 3. exp. | | non-Newtonian fluid $q = -0.2$ | | | | domain size |
|---|---|---|---|---|---|---|
| mesh | $\Delta t$ | $Err(\boldsymbol{v}_h)$ | EOC$(\boldsymbol{v}_h)$ | $Err(\eta_h)$ | EOC$(\eta_h)$ | $\lvert\Omega(\eta_{h/2})\rvert$ |
| 2/1 | 0.002 | 1.404563 | | 0.047666 | | 3.220798 |
| 3/2 | 0.002 | 0.2561264 | 2.455 | 0.014985 | 1.669 | 3.211087 |
| 4/3 | 0.002 | 0.03979248 | 2.686 | 0.010263 | 0.546 | 3.208564 |

Table VII. Convergence order in deforming tube

| 3. exp. | | Newtonian fluid $q = 0$ | | | | domain size |
|---|---|---|---|---|---|---|
| mesh | $\Delta t$ | $Err(\boldsymbol{v}_h)$ | EOC$(\boldsymbol{v}_h)$ | $Err(\eta_h)$ | EOC$(\eta_h)$ | $\lvert\Omega(\eta_{h/2})\rvert$ |
| 2/1 | 0.002 | 1.199429 | | 0.066524 | | 3.251774 |
| 3/2 | 0.002 | 0.2391076 | 2.327 | 0.017199 | 1.952 | 3.239012 |
| 4/3 | 0.002 | 0.05107463 | 2.227 | 0.007592 | 1.180 | 3.236897 |

with grid refinement. The reason for decreasing the convergence order of $\eta$ in the 3. experiment (Dirichlet boundary condition at the central line) is the decreasing of the convergence of pressure, which is particularly the force for domain deformation. The Table VIII shows the comparisons of EOC for complete solution (velocity and pressure $p$) $\boldsymbol{u} = (\boldsymbol{v}, p)$ for both experiments 2. and 3. We can conclude, that the symmetry boundary condition are better for preserving the convergence for pressure and consequently the domain deformation $\eta$, on the other hand the Dirichlet boundary condition helps to achieve the 2. order convergence for velocity.

Table VIII. Comparisons of EOC in rigid tube for both experiments: with Dirichlet boundary condition and symmetry condition at the central line

| non-Newtonian fluid $q = -0.20$ | | 2. experiment symmetry condition | | 3. experiment Dirichlet condition | |
|---|---|---|---|---|---|
| mesh | $\Delta t$ | $Err(\boldsymbol{u}_h)$ | EOC | $Err(\boldsymbol{u}_h)$ | EOC |
| 2/1 | 0.002 | 37.2222 | | 108.8875 | |
| 3/2 | 0.002 | 7.708046 | 2.272 | 24.44905 | 2.155 |
| 4/3 | 0.002 | 1.581982 | 2.285 | 12.07363 | 1.018 |

## 8. CONCLUSIONS

In this paper we have simulated blood flow in a part of elastic vessel and analyzed some hemodynamical control quantities. We have modeled blood as a shear-thinning non-Newtonian fluid and chosen two well-known models, the Carreau (or Carreau-Yasuda) model and the Yeleswerapu model. Comparisons with the Newtonian model are presented as well. We compared the wall deformation and the hemodynamical wall parameters, the wall shear stress $WSS$ and the oscillatory shear index $OSI$ for a straight and stenotic tube.

The fluid equations were approximated by the finite volume method with the pseudo-compressibility stabilization for spatial discretization. We have linearized the non-linear Cauchy stress tensor by fixed point iterations. For the deformation equation we used the Newmark scheme and the finite difference scheme. The global iterations with respect to the domain geometry are based on the ALE formulation and on the decoupling of the fluid and structure. Numerical experiments indicate, that the global iterative method is robust and relatively fast. The stability and accuracy of numerical method have been tested for several model parameters, including the physiological parameters for shear dependent viscosity and inflow rate.

The presented results demonstrate a significant influence of the non-Newtonian fluid model, especially for hemodynamical control quantities such as the $WSS$ and $OSI$. Larger negative absolute values of $WSS$ appears in the case of non-Newtonian fluids modeled with physiological viscosities. According to some authors this indicates the appearance of recirculation zones and reversal flows around stenosis, which seems to be better predicted by the non-Newtonian models. Further, the domain geometry has also a considerable influence on the wall deformation as well as on the $WSS$ and $OSI$. Moreover the maximum values of $OSI$ are larger for the non-Newtonian models in comparison to the Newtonian flow. Such high $OSI$ values at the end of stenotic occlusion indicate a large oscillatory nature of the wall shear stress and could yield further to additional stenotic plug.

Experiments for physiological viscosities have been performed as well. We have shown that for higher Reynolds numbers the effect of non-Newtonian

rheology are even more profound. All results confirm a significant influence of the fluid rheology and domain geometry on the wall deformation as well as on the hemodynamics wall parameters.

In future we want to extend the model and consider the generalized Oldroyd-B model that includes the viscoelastic properties of blood as well. Additionally, we want to consider more complex vessel geometries, e.g. bifurcations. Thus, we will not restrict ourselves only to the deformation in one direction but consider the domain deformation in both $x_1$ and $x_2$ direction, $\eta = (\eta_1, \eta_2)$. An important point of numerical simulation is a correct outflow boundary condition, reflecting the influence of the rest of the circulatory system. According to the [23] this can be realized by so-called impedance condition arising from coupling the model with some less dimensional model (1D or 0D lumped model).

The theoretical analysis of similar problems for Newtonian fluids in a moving domain is studied e.g., in [24], [9], [4], [22], etc. Theoretical results of existence and uniqueness of the weak solution to our shear-dependent non-Newtonian fluid-structure problem have been presented in Section 4. In [12] however only the existence and uniqueness of the solution for one global iteration has been shown. The convergence of global iterative method has been shown only for a special case in [6]. Our future goal is to show the convergence of global iterations, whose convergence is indicated by our numerical experiments.

## ACKNOWLEDGEMENTS

This research has been financed by the European Union's 6th Framework Programme Reference under the Contract no. DEASE: MEST-CT-2005-021122. The authors gratefully acknowledge this support. The first author would like to thank Adélia Sequeira (Instituto Superior Téchnico, Lisbon) for fruitful discussions.

## REFERENCES

1. Bastian P, Johannsen K, Reichenberger V : *UG tutorial*, 2001
2. Broser PhJ : *Simulation von Strömungen in Blutgefässen*, Master's thesis, Ruprechts-Karl University, Heidelberg, 2001
3. Čanič S : Blood flow through compliant vessels after endovascular repair: Wall deformations induced by the discontinuous wall properties, Comput. Vis. Sci. 4 (2002), 147–155
4. Chambolle A, Desjardin B, Esteban MJ, Grandmont C : Existence of weak solutions for unsteady fluid-plate interaction problem, J. Math. Fluid Mech. 7 (3) (2005), 368–404
5. Černý J : *Numerical modelling of non-Newtonian flows with application in hemodynamics*, PhD thesis, in preparation
6. Filo J, Zaušková A : 2D Navier-Stokes equations in a time dependent domain with Neumann type boundary conditions, J. Math. Fluid Mech. 10 (2008), 1–46
7. Formaggia L, Gerbeau JF, Nobile F, Quarteroni A : On the coupling of 3D and 1D Navier-Stokes equations for flow problems in compliant vessels, Computer Methods in Applied Mechanics and Engineering 191 (6-7) (2001), 561–582
8. Gijsen FJH, van de Vosse FN, Jansen JD : Influence of the non-Newtonian properties of blood flow on the flow in large arteries: steady flow in a carotid bifurcation model, Journal of Biomechanics 32 (1999), 601–608
9. Guidorzi M, Padula M, Plotnikov PI, Bellomo N : Hopf solutions to a fluid-elastic interaction model, Mathematical Models and Methods in Applied Sciences 18 (2) (2008), 215–270

10. Kröger T, Lukáčová-Medviďová M : An evolution Galerkin scheme for the shallow water magnetohydrodynamic equations in two space dimensions, Journal of Computational Physics 206 (2005), 122–149
11. Lukáčová-Medviďová M, Černý J : Numerical modelling of non-Newtonian shear-thinning viscoelastic fluids with application in hemodynamics, Proceedings of the Second International Symposium Modelling of Physiological Flows, Portugal, (ed. Sequeira et al.), 2005
12. Lukáčová-Medviďová M, Zaušková A : On the existence and uniqueness of non-Newtonian shear-dependent flow in compliant vessels, submitted 2008
13. Nadau L, Sequeira A : Numerical simulations of shear dependent viscoelastic flows with a combined finite element - finite volume method, Computers and Mathematics with Applications, to appear
14. Nägele S : *Mehrgitterverfahren für incompressiblen Navier–Stokes Gleichungen im laminaren und turbulenten Regime unter Berücksichtigung verschiedener Stabilisierungsmethoden*, PhD thesis, Ruprechts-Karl University, Heidelberg, 2003
15. Nobile F : *Fluid-structure interaction problems in hemodynamics*, Master's thesis, Technical University in Milan, 1998
16. Quarteroni A : Fluid-structure interaction for blood flow problems, (In Lecture notes on Simulation of Fluid and Structure Interaction, AMS-AMIF Summer School, Prague), European Mathematical Society, 2001
17. Perktold K, Rappitsch G : Mathematical modelling of local arterial flow and vessel mechanics, Comput. Methods for Fluid-Structure Interaction (1994), 230–245, Longman, Harlow
18. Quarteroni A : Mathematical and numerical simulation of the cardiovascular system, In Proceedings of the ICM,3 (2002), 839–850, Beijing
19. Quarteroni A, Gianluigi R : Optimal control and shape optimization of aorto-coronaric bypass anastomoses,$M^3$ AS, Mathematical Models and Methods in Applied Sciences 23 (12) (2003), 1801–23
20. Quarteroni A, Formaggia L : Mathematical modelling and numerical simulation of the cardiovascular system, Handbook of Numerical Analysis (P.G Ciarlet and J.L Lions Eds.), Elsevier, Amsterdam, 2002
21. Rajacopal K, Lawson J : Regulation of hemostatic system function by biochemical and mechanical factors, Modeling of Biological Materials, Series: Modeling and Simulation in Science, Engineering and Technology, Birkhäuser, Boston (2007), 179–201
22. Surulescu C : The instationary moion of a Navier-Stokes fluid through a vessel with an elastic cover, IWR Preprint, University of Heidelberg, 2005
23. Taylor ChA, Vignon-Clementel IE, Figueroa CA, Jansenca, KE : Outflow boundary conditions for three-dimensional finite element modeling of blood flow and pressure in arteries, Comput. Methods Appl. Mech. Engrg. 195 (2006), 3776–3796
24. Beirao da Veiga H : On the Existence of Strong Solution to a Coupled Fluid-Structure Evolution Problem, J. Math. Fluid Mech. 6 (1) (2001), 21–52
25. Yeleswarapu KK, Kameneva MV, Rajagopal KR, Antaki JF : The flow of blood in tubes: theory and experiments, Mech. Res. Comm. 25 (3) (1998), 257–262
26. Zauskova A : *2D Navier–Stokes equations in a time dependent domain*. PhD thesis, Comenius University, Bratislava, 2007